RSC Pharmaceutics

ROYAL SOCIETY OF CHEMISTRY

PAPER

View Article Online
View Journal | View Issue

Check for updates

Cite this: *RSC Pharm.*, 2025, **2**, 163

Dual-action antimicrobial surface coatings: methylene blue and quaternary ammonium cation conjugated silica nanoparticles†

Haritha Kirla, *[a,b] Juliana Hamzah, [b] Zhong-Tao Jiang [a] and David J. Henry *[a]

Received 26th September 2024,
Accepted 28th November 2024

DOI: 10.1039/d4pm00278d

rsc.li/RSCPharma

The increasing prevalence of healthcare-associated infections from multidrug-resistant bacteria presents a growing challenge due to their high transmissibility, and resistance to traditional antimicrobial strategies. In this study, we introduce an innovative dual-mode antibacterial strategy through the development of novel surface coatings on glass substrates, offering a proof-of-concept solution for enhanced infection control. Our approach uniquely combines the light-active methylene blue silane (MBS1) dye with the potent antimicrobial compound dimethyloctadecyl[3-(trimethoxysilyl)propyl] ammonium chloride (QAS) into silica nanoparticles (SNPs) to create multifunctional antibacterial surface coatings. The distinct use of silane-functionalized MB and QA enables strong covalent bonding with silica nanoparticles, while the robust silane chemistry ensures durable adhesion of SNPs to the glass substrates. While MBS1–SNP coatings generated highly hydrophilic (CA = 28°), light-active surfaces, combination of QAS (QA–MBS1–SNP) coating enhanced surface hydrophobicity (CA = 90°) without compromising photokilling efficiency. The antibacterial efficacy of these coatings was rigorously tested against the Gram-negative bacterium *Escherichia coli*. The synergistic action of MB and QA demonstrated exceptional photokilling performance achieving >99.999% (>5-log reduction) bactericidal activity under white light (~500 lux, ~0.0732 mW cm^{-2}) and effectively inhibited biofilm formation by up to 80%. The demonstrated efficacy of these coatings highlights their potential for transformative applications in healthcare settings, providing a robust, multifaceted approach to infection control.

1. Introduction

Hospital acquired infections (HAIs) pose a grave and imminent global threat that demands immediate attention. The impact of HAIs is staggering, affecting millions of patients globally. In Australia alone, public hospitals witness an annual occurrence of approximately 170 600 HAIs, resulting in ~7600 deaths.[1] Moreover, these infections contribute to a prolonged hospital stay, averaging 18 days longer compared to patients without HAIs.[2,3] These infections are a significant challenge for both society and health care organizations, causing a financial burden of billions of dollars for governments. HAIs are mainly caused by multi-drug resistant pathogens, transmitted through contaminated surfaces on medical equipment and implants such as catheters and ventilators, and intensified by excessive antibiotic use. The recent advent of the COVID-19 pandemic has further exacerbated this issue, particularly associated with the use of ventilators.[4] This has elevated the imperative need for innovative methods for creating antibacterial materials and surface coatings.

The utilization of antibacterial surface coatings has emerged as a promising avenue, particularly those loaded with antibiotics capable of impeding the attachment and progression of biofilms. However, the rising prevalence of antibacterial-resistant bacteria has underscored the need to explore alternative modes of action, distinct from conventional antibiotics.[5–10] Antibacterial photodynamic therapy (*a*PDT) is one of the alternative approaches for treating microorganisms resistant to traditional antibiotics.[11] The *a*PDT strategy involves the synergistic interplay of light and a photosensitizing agent, to induce a photochemical reaction that eradicates bacteria by generating toxic reactive oxygen species.[12] Distinguished by numerous advantages over traditional antibiotics, *a*PDT demonstrates a broad spectrum of action, proving effective against diverse organisms.[7,11] Notably, its immediate bactericidal action significantly reduces the risk of resistance development, as it targets multiple cellular components.

[a]*Chemistry and Physics, College of Science, Technology, Engineering and Maths, Murdoch University, WA 6150, Australia. E-mail: David.henry@murdoch.edu.au*
[b]*Targeted Drug Delivery, Imaging & Therapy Laboratory, Harry Perkins Institute of Medical Research, The University of Western Australia, Centre for Medical Research, Nedlands, WA 6009, Australia. E-mail: Haritha.kirla@perkins.org.au*

†Electronic supplementary information (ESI) available: The schematic illustration of glass substrate preparation and surface coatings and diagrammatic representation of bactericidal activity test with coated surfaces. See DOI: https://doi.org/10.1039/d4pm00278d

A surface coating incorporating *a*PDT represents an innovative approach to combat bacterial infections. While research has delved into surface coatings containing metal nanoparticles, such as Ag_n and Cu_n, for the creation of light-active coatings, reports indicate severe toxic effects associated with these materials.[9] In contrast, organic synthetic dyes, serving as photosensitizers (PSs), have proven to be more effective against multi-drug resistant bacteria.[13,14] Among these dyes, methylene blue (MB) has garnered significant attention for its *a*PDT activity in clinical settings. The cationic charge of MB facilitates high affinity for binding to bacterial cell walls, enhancing its effectiveness.[15] Numerous studies have demonstrated the excellent activity of MB against planktonic bacteria.[16] Recent research has showcased MB's efficacy as an *a*PDT disinfectant against coronavirus-contaminated personal protective equipment.[17] Furthermore, Ghareeb *et al.*,[8] integrated MB with a UV-photocrosslinkable polymer, creating photodynamic coatings for infection control.

The integration of PSs with nanotechnology has been shown to significantly influence the outcome of PDT.[5] Nanoparticles serve a dual purpose by acting as a secure carrier for PSs and shielding them from excessive photobleaching. In addition, they contribute to the improved safety profile and biocompatibility of PSs, mitigating potential dark toxic effects. Furthermore, nanoparticles play a pivotal role in enhancing the interaction between PSs and bacterial walls due to their unique surface chemistry.[9,18] In the context of surface coatings, nanoparticles facilitate the infusion of PSs into coating materials, enhancing their overall efficacy.[16] While numerous studies have underscored the augmented anticancer PDT efficacy achieved through PS encapsulation with nanoparticles,[18] research in the domain of *a*PDT remains relatively scarce. Among the diverse array of nanoparticles, silica nanoparticles stand out as particularly noteworthy. Their proven biocompatibility, versatility with tuneable morphology, and flexible surface chemistry make them ideal candidates for facilitating advancements in *a*PDT.[19,20]

Many research works have documented the immobilization of free MB onto silicone supports, predominantly employing the swell-shrink method.[6] However, a notable drawback of this approach is the potential leaching of the dye from the test surfaces upon incubation with solutions.[7] As an alternative, the conjugation of MB onto the silicone support presents a viable solution to eliminate this issue. Nevertheless, MB lacks a supporting functional group for direct covalent conjugation to the silicone support. Piccirillo *et al.*,[21] demonstrated the conjugation of toluidine blue O to an activated silicone polymer through an amide linkage. Despite this progress, there remains a dearth of reported works concerning the utilization of MB-conjugated silica nanoparticles in the context of *a*PDT surface coatings. This unexplored avenue holds promise for addressing the limitations associated with dye leaching, potentially opening new frontiers in the development of surface coatings with enhanced stability and performance. Furthermore, quaternary ammonium compounds have demonstrated remarkable efficacy as antibacterial and antibiofouling agents.[22] They disrupt bacterial cell membranes, leading to leakage of cellular contents and ultimate cell death.[23,24] Additionally, their positive charge facilitates adherence to microbial surfaces, making them effective in preventing biofilm formation.

Although both methylene blue (MB) and quaternary ammonium ions have been extensively studied for their antibacterial properties, to the best of our knowledge, there are no reports on their combined use for synergistic antibacterial applications. We hypothesize that integrating MB with quaternary ammonium compounds could offer a novel approach by combining two distinct mechanisms of action: MB's oxidative damage to bacteria under light exposure and quaternary ammonium ion offers prolonged antibacterial effects through membrane disruption. This synergistic approach could be more effective than using either agent alone, addressing both initial infection control and long-term antimicrobial activity.

The present work demonstrates the development of these dual-functional surface coatings on glass substrates through the application of MB and a quaternary ammonium compound covalently conjugated to SNPs, combined with the spin coating method. The synthesized nanoparticles and subsequently developed surface coatings were characterized for morphology by electron microscopy and optical properties by UV-Vis spectral analysis. The newly developed surface coatings were tested for *a*PDT efficacy and biofouling activity against *Escherichia. coli* (*E. coli*) microorganism in both dark and low-level white light exposure at ambient temperatures.

2. Materials

2.1. Chemicals

Tetraethylorthosilicate (TEOS, 78-10-4, reagent grade 98%, Sigma-Aldrich) and dimethyloctadecyl [3-(trimethoxysilyl) propyl] ammonium chloride (QAS, 27668-52-6, 42 wt% in methanol, Sigma-Aldrich) were obtained from Merck, Australia. 25% w/v ammonium hydroxide (NH_4OH, 1336-21-6, AR grade, Ajax Fine Chem) and absolute ethanol (AR grade, 99.5%) supplied by MCScientific, Australia were used as received. Nutrient broth powder was purchased from Southern Biological (Alphington, Victoria, Australia). EM grade glutaraldehyde 25% aqueous solution was purchased from ProSciTech (product code: C002), Australia. Millipore filtered deionised water purified with a Milli-Q system, and sterilized phosphate buffered saline (1× PBS), made in-house were used throughout the experimental work. An alkoxy silane derivative of methylene blue 3-(dimethylamino)-7-(methyl(3-(trimethoxysilyl) propyl)amino) phenothiazin-5-ium triiodide (MBS1) was prepared in the lab according to our previous reported method.[25]

2.2. Bacterial strain and growth conditions

Gram negative *E. coli* [(Migula 1895) Castellani and Chalmers 1919] strain (kindly donated by Microbiology teaching preparation lab, Murdoch University) was used in this study as a model organism. The bacterial culture was subcultured in Nutrient Broth (NB) media at 37 °C overnight in an orbital

shaker at 200 rpm. Prior to each experiment, the optical density (OD) of the overnight inoculum was adjusted to 0.5 McFarland standard (~1.5×10^8 CFU mL^{-1}) in PBS. This was further diluted in 1× PBS to obtain a bacterial working solution with ~10^5 CFU mL^{-1}. All experiments were performed at this concentration.

3. Instrumentation

Transmission electron microscope (TEM) (JEOL F200 FEGTEM, JEOL Ltd, Tokyo, Japan) was used to measure the nanoparticle size, shape, and surface morphology of the bacteria. Zeta potential and hydrodynamic radius of the nanoparticles were analyzed using Zetasizer NanoZS (Malvern Inst., Malvern, UK). A scanning electron microscope (SEM) (JEOL-JCM-6000 benchtop model, JEOL Ltd, Tokyo, Japan) equipped with energy dispersive X-ray spectroscopy (EDS) and operating at 15 kV was used to investigate the nanoparticle coated glass surfaces and to record the information regarding the elemental composition of the coated surfaces. Zeiss 1555 VP-FESEM (Carl Zeiss, Germany) at 5 kV was used to check biofilm formation on the coated glass surfaces, and to investigate the extracellular features and morphology changes of bacterial biofilms before and after PDT treatment.

A PerkinElmer Lambda 650 UV-Visible spectrophotometer (PerkinElmer, Inc., USA) was used to collect the UV-Visible spectral data of nanoparticle coated surfaces. The measurements were conducted over a spectral range of 250 to 800 nm in 2 nm increments. The base line correction was obtained using an uncoated glass slide as a reference. BioTek PowerWave XS2 (BioTek Instruments, Inc., Vermont, USA) microplate reader and Shimadzu UV-2600 (Shimadzu Corporation, Kyoto, Japan) UV-Visible spectrophotometers were used to run UV-Vis spectral measurements and OD of bacterial samples. Nikon C2+ (Nikon Instruments Inc., Japan) confocal microscope was used for fluorescence imaging.

4. Experimental methods

4.1. Synthesis of silica nanoparticles for surface coatings

The sol–gel process was used in the synthesis of various types of silica nanoparticles (SNPs) reported in this work.

The standard synthesis procedure for SNPs involved the addition of 5 mL (22.4 mmol) of TEOS to a solution containing 10 mL of ethanol, 0.5 mL (8.2 mmol) of 28% w/v NH_4OH, and 1.2 mL of water. This mixture was stirred for 4 hours at room temperature to form a sol. The sol was then aged overnight at room temperature and utilized for surface coating preparations.

To produce quaternary ammonium cation conjugated SNPs (QA–SNP), 2.5 mL (11.2 mmol) of TEOS and 2.5 mL (2.1 mmol) QAS were added to ethanol (10 mL), water (1 mL), and 28% w/v NH_4OH (0.5 mL, 8.2 mmol). The mixture was stirred for 4 hours, followed by aging overnight to form QA–SNP, which was then used in surface coatings.

MBS1 covalently conjugated SNP (MBS1–SNP) was synthesized using our previously prepared MBS1 derivative. The synthesis of these particles followed the standard procedure with the inclusion of 0.5 mg (1 μmol) of MBS1 added during the addition of TEOS to facilitate co-condensation with TEOS.[26]

For the synthesis of dual functionalized QA and MBS1 conjugated SNPs (QA–MBS1–SNP), a mixture of MBS1 (1 μmol), TEOS (11.2 mmol), and QAS (2.1 mmol), was added to ethanol (10 mL), water (1.2 mL), and NH_4OH (0.5 mL) mixture. The mixture was stirred for 4 hours, followed by aging overnight.

After synthesis, batches of nanoparticles were isolated for characterization, using centrifugation at 15 000 rpm, followed by successive washes with water and ethanol. The samples were then subjected to freeze-drying.

4.2. Surface coating preparation

The preparation of the glass substrates and the subsequent surface coating procedures followed the process outlined in SFig. 1A.†

Prior to the coating process, thorough cleaning of the glass substrates was undertaken to ensure the creation of homogenous and uniform coatings. Initially, the glass substrates (25 × 25 mm) were rinsed with deionised water, accompanied by 15 minutes of sonication in water and acetone. Subsequently, the substrates underwent sonication at 40 °C for 30 minutes in a 1 M potassium hydroxide solution (KOH). This was repeated then the substrates were soaked in 1 M KOH for 12 hours. Between each sonication step, the substrates were washed three times with deionized water. Finally, the cleaned slides were dried in a vacuum oven at 50 °C for 20 minutes.

The cleaned glass slides were then employed for spin coating using a Polos spin coater, following the steps outlined in SFig. 1B,† with nanoparticle solutions used for surface coatings.

The following parameters were used in the spin coating process. Firstly, ~100 μL of the nanoparticle solution, prepared previously (described in 4.1) was dispensed over 10 seconds onto a glass substrate spinning at 500 rpm. To achieve spreading of the solution the speed of rotation was increased to 1000 rpm for 20 seconds. Initial drying was achieved by spinning the coated substrate at 2000 rpm for 20 seconds. The coated sample was then further dried on a hot plate at 100 °C for 5 minutes. This coating process was repeated three times. After the final coating, the resultant coated glass substrates were left to dry overnight under vacuum at 50 °C.

To assess hydrophilicity and wettability, 10 μL water droplets were placed onto the surfaces. The droplets are photographed immediately and contact angles were measured by Image J software using low bond axis symmetric drop shaped analysis.

4.3. Light source

A primary white LED (Light Emitting Diode) (12 Watt) with a lux value of approximately 500–600 lux, placed at one meter from samples, was used as a light source for all *a*PDT experiments.

4.4. Bactericidal activity of coated surfaces

The bactericidal efficacy of various coated surfaces, in both light and dark conditions, was assessed against *E. coli* following an established protocol.[27] Briefly, 30 μL of a bacterial suspension (1.5×10^8 CFU mL^{-1}) was inoculated onto uncoated, SNP, QA–SNP, MBS1–SNP, and QA–MBS1–SNP coated glass surfaces. One set of test samples was placed in a Petri dish within a humidified chamber at 25 °C under dark conditions, while the other set was exposed to the LED light source with an intensity of ~500 lux, to evaluate *a*PDT efficacy of the coated surfaces as shown in SFig. 2.† After a 30 minute exposure period, bacterial-treated surfaces were thoroughly rinsed with 2 mL of PBS to collect bacteria. Subsequently, 20 μL of the bacterial suspension was subcultured on agar plates to enumerate viable bacteria. Each experiment was conducted in triplicates, and results were expressed as the mean.

4.5. Transmission electron microscopy (TEM) imaging

The impact of *a*PDT on the surface morphology of the bacterial culture was evaluated using TEM imaging. Initially, the test bacterial culture was treated with the coated surfaces as described above. The treated bacteria were then collected through centrifugation and fixed in 2.5% glutaraldehyde followed by 1× PBS wash, twice.

Approximately 5 μL of the bacterial suspension was dropped on a continuous Cu grid and allowed to stand for one hour. Subsequently, excess solution was carefully absorbed with the help of a filter paper. The fully dried grids were then subjected to imaging using JEOL F200 FEGTEM (JEOL Ltd, Tokyo, Japan), at the Centre for Microscopy, Characterisation and Analysis, University of Western Australia. The instrument was operated at an accelerating voltage of 200 kV and magnifications ranging from 40 000× to 80 000×. Images were processed by ImgeJ software.

4.6. Growing biofilms on the nanoparticle coated glass surfaces

The biofilm inhibition potential of uncoated, SNP, QA–SNP, MBS1–SNP, and QA–MBS1–SNP coated glass surfaces was investigated through a comprehensive assessment.

50 μL of bacterial suspension (10^5 CFU mL^{-1}) was dispensed onto the coated glass surfaces and covered with culture media. A set of samples were maintained in the dark for 48 hours to allow biofilm formation, while another set was continuously exposed to white light during biofilm formation (48 hours). Subsequently, matured biofilms were washed carefully from the slides to remove planktonic bacteria. Uncoated glass slides were used as a control.

The quantification of biofilms, derived from the aforementioned methodology, was performed employing the crystal violet assay, as outlined by Paramanantham *et al.*,[28] with minor adjustments. Firstly, the biofilms grown on the nanoparticle coated surfaces in dark and in white light conditions were washed gently with 1× PBS to remove unattached bacteria. Then, approximately 200 μL of a 0.1% w/v crystal violet solution was added on coated glass surfaces. The samples were incubated for 15 minutes, followed by a thorough wash with 1× PBS. After allowing complete drying, ethanol was utilized to extract the crystal violet bound to the bacteria cells. Subsequently, the OD was measured at 585 nm, providing a quantitative assessment of biofilm formation. All experiments were performed as triplicates and the results were expressed as mean.

4.7. Scanning electron microscopy (SEM) imaging

The morphology of the coated glass surfaces were visualized using SEM (JEOL-JCM-6000, JEOL Ltd, Tokyo, Japan), at Murdoch University. The instrument was operated at 15 kV at a magnification from 500× to 550×. Elemental mapping was performed using an integrated energy dispersive X-ray spectroscopy detector.

The biofilms contained glass substrates from the above-mentioned experiment, along with control experimental slides (refer to section 4.6), were fixed in 2.5% glutaraldehyde for 10 minutes, followed by gradient ethanol fixation (50%, 75%, and 100%) for 10 minutes each. Subsequently, the slides were dried and sputter-coated with a 10 nm layer of platinum. Biofilm formation was visualized using Zeiss 1555 VP-FESEM (Carl Zeiss, Germany) (Centre for Microscopy, Characterisation and Analysis, University of Western Australia), operated at an accelerating voltage of 5 kV, 6.8 to 6.9 mm working distance, and magnifications ranging from 10 000× to 20 000×.

4.8. Fluorescence imaging of biofilms

Additional fluorescence imaging was performed using biofilms developed on the glass substrates as outlined in section 4.6. The biofilms were fixed with 2.5% glutaraldehyde for 10 minutes followed by staining with acridine orange (AO) (2 μg mL^{-1}) for 15 min at room temperature. Fluorescence imaging was then performed using a Nikon C2+ confocal microscope at 525 nm.

4.9. Statistical analysis

Statistical analysis was conducted using GraphPad Prism 10 (GraphPad Software, San Diego, CA, USA). A two-tailed Student's *t*-test was used to compare groups. For comparisons involving more than two groups, one-way ANOVA followed by Tukey's *post-hoc* test was used. Statistical significance was determined with the following thresholds: $*p < 0.05$, $**p < 0.01$. Data are presented as mean ± Standard Error of the Mean (SEM), with error bars indicating SEM.

5. Results and discussion

5.1. Synthesis of SNP, QA–SNP, MBS1–SNP, and QA–MBS1–SNP and their characterization

The synthesis of these nano-formulations was achieved through the sol–gel methodology. TEOS was utilized as the metal precursor across all nanoparticle types. QAS and MBS1 were employed to introduce quaternary ammonium cation

(QA) and MB modifications to the nanoparticle surfaces, respectively. The silane functional groups present on QAS and MBS1 facilitated their covalent conjugation to the SNPs. In the reaction, the silane compounds underwent hydrolysis and condensation in the presence of water and NH_4OH, forming a sol–gel mixture. This sol–gel mixture was then either directly applied onto glass surfaces to create the corresponding surface coatings or isolated to collect nanoparticles for characterization.

Characterization of these resulting nanoparticles encompassed assessments of their size and zeta potential. TEM imaging revealed the monodisperse nature of the spherical nanoparticles, with sizes ranging from 5–10 nm (Fig. 1). Comprehensive results are presented in Table 1, indicating that all nanoparticle types were obtained in ultra-small sizes.

Zeta potential values determined in water were negative for both SNP and MBS1–SNP, with values of −34 ± 0.85 mV and −13.5 ± 2.9 mV, respectively (Table 1). The negative values were attributed to the presence of electronegative hydroxyl groups on the surfaces of the nanoparticles. The negative surface charge of MBS1–SNP was lower than that of SNP, possibly due to the presence of cationic MB molecules on the particle surfaces, which partially offset the negative charge of the hydroxyl groups. On the other hand, both QA–SNP and QA–MBS1–SNP displayed positive zeta potential (Table 1) due to the positive charge of QA groups present on the surface of the particles.

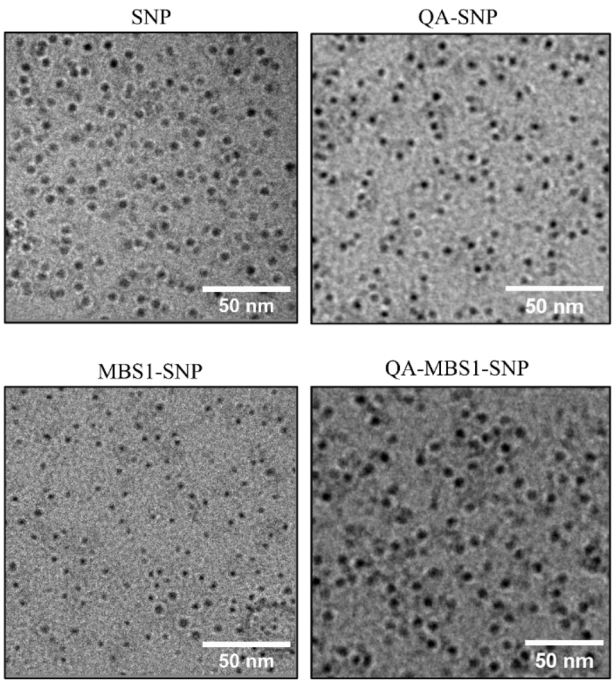

Fig. 1 TEM images of spherical monodispersed silica nanoparticles (SNPs) functionalised with quaternary ammonia groups (QAS) and methylene blue (MBS1) dye (scale bar 50 nm).

Table 1 Characteristics of silica nanoparticles and SNP coatings

Sample name	Size[a] (nm ± SD)	Zeta potential[b] (mV ± SD)	Contact angle[c] (°)
SNP	5.4 ± 0.5	−34.0 ± 0.8	41
QA–SNP	5.8 ± 0.7	+33.5 ± 1.5	102
MBS1–SNP	6.4 ± 0.8	−13.5 ± 2.9	28
QA–MBS1–SNP	6.9 ± 0.6	+25.2 ± 1.1	90

[a] Particle size was based on TEM imaging of more than 200 particles chosen randomly. [b] Zeta potential measurements in water (0.1 mg mL^{-1}). [c] Contact angle (CA) measurements for water droplets.

5.2. Synthesis of dual functional light active surface coatings

The development of SNP, QA–SNP, MBS1–SNP, and QA–MBS1–SNP coated surfaces was achieved utilizing the spin coating method. This technique was selected for its simplicity, enabling the production of thin and uniform coatings on glass substrates.[29] Sol–gel synthesis of nanoparticle solutions was employed to provide control over film thickness, making it a preferred method for generating oxide coatings on glass substrates.[30] Additionally, sol–gel spin coating is well-suited for research applications.

As described in SFig. 1A,† glass slides underwent an initial etching process in a 1 M KOH solution to expose hydroxyl groups for crosslinking with silane groups.[31] The spin coating process was iterated three times to achieve the desired thickness, interspersed with 5 minute drying intervals at 100 °C between each coating, to enhance the condensation process. Following spin coating, the resulting thin films underwent overnight curing at 75 °C under vacuum conditions to ensure thorough drying. This procedure also promoted siloxane condensation, enabling hydrolyzed silane groups on nanoparticles to effectively condense with hydroxyl groups on the glass surface (Fig. 2). This drying stage is crucial for establishing robust siloxane bonds between the etched glass substrate surface and the nanoparticles,[32,33] while the vacuum environment serves to prevent any potential formation of cracks in the coated surfaces.[34]

Fig. 2 presents contact angle (CA) images of uncoated, SNP, QA–SNP, MBS1–SNP, and QA–MBS1–SNP coated surfaces, with contact angle results detailed in Table 1. CA is an important parameter to evaluate the water repelling capacity of the surfaces, which in turn is useful in the determination of repellence and inhibition of biofilm formation. Contact angles less than 90° indicate the surface wettability is high. The uncoated, SNP, and MBS1–SNP coated surfaces exhibited CAs 55°, 41°, and 28°, respectively, confirming their hydrophilic nature. The CA for uncoated glass closely resembled the findings of Sriramulu *et al.*,[35] (55.7°), while the CA decreased to 41° after SNP coating. These values were lower than those reported by Zainuri *et al.*,[36] (70°) for SNP-coated surfaces, which could be attributed to differences in SNP particle sizes used in surface coatings. Zainuri *et al.* utilized SNP particles of ~1 μm, whereas this study employed SNP particles ≤10 nm, with smaller particles offering increased surface area and a higher number of hydroxyl groups, thereby enhancing hydrophilicity. Conversely, QA–SNP and QA–MBS1–SNP coated surfaces displayed CAs of 102° and 90°, indicating their hydrophobic nature. These findings were consistent with those reported by

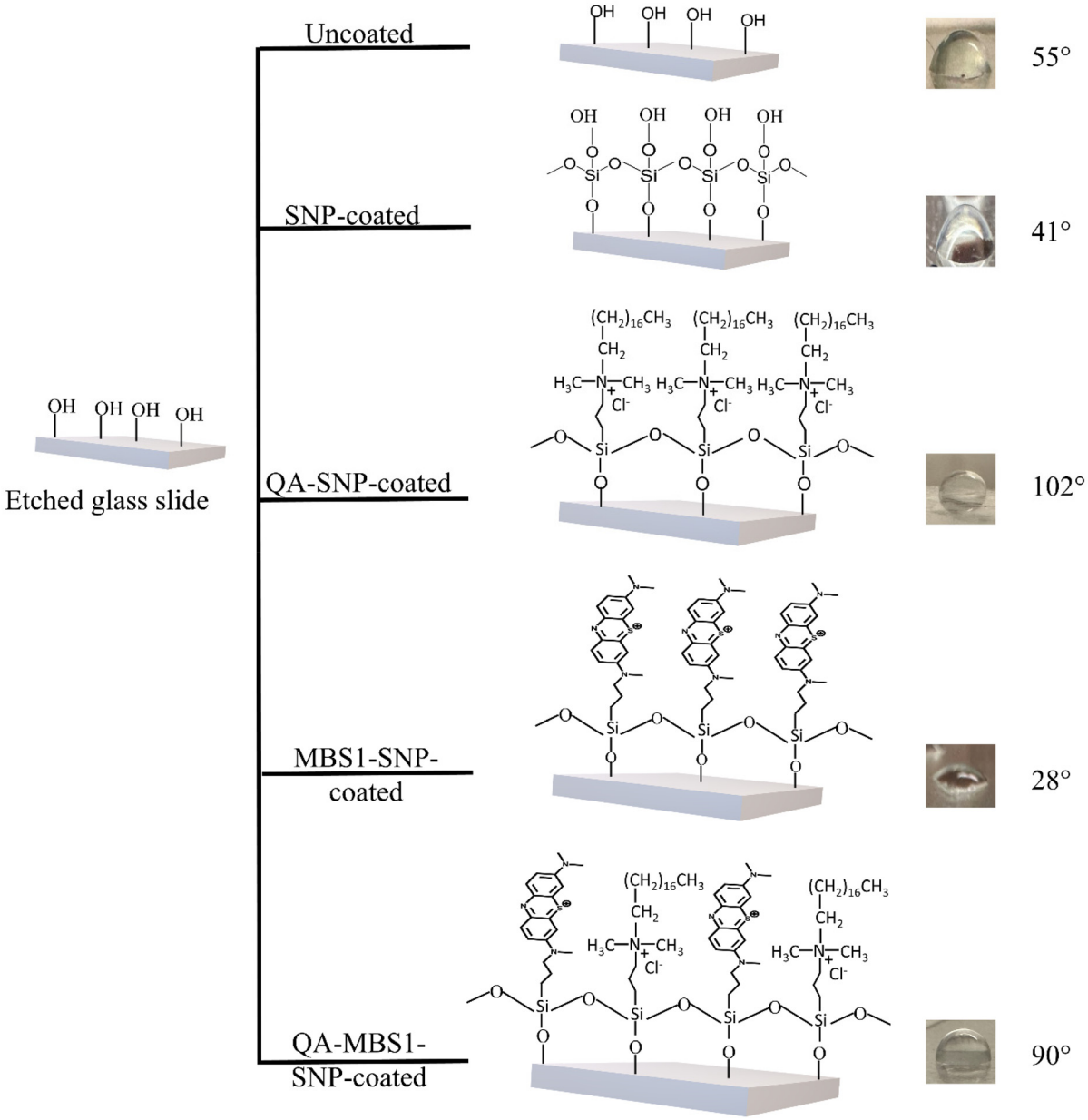

Fig. 2 Schematic illustration of uncoated, SNP, QA–SNP, MBS1–SNP, and QA–MBS1–SNP coated glass surfaces and respective water contact angle measurements. QA–SNP and QA–MBS1–SNP coated surfaces showed water contact angle ≥90°, indicating hydrophobic surfaces.

Lou *et al.*,[37] for quaternary ammonium functionalized surfaces (CA = 105° ± 2). The hydrophobicity observed in these glass surfaces can be attributed to the presence of QA groups on the nanoparticle surfaces, with the octadecyl alkyl chain on the QA contributing to surface hydrophobicity.

The SEM images presented in Fig. 3A depict the surface morphology of uncoated, SNP, QA–SNP, MBS1–SNP, and QA–MBS1–SNP coated surfaces. The uncoated surface appears smooth, as do the SNP and MBS1–SNP coatings. However, the QA–SNP and QA–MBS1–SNP coated surfaces exhibit roughness characterized by irregular patterns, likely due to the presence of long alkyl chains modified on the surface of the SNPs. Interestingly, the QA–MBS1–SNP coating displays a smoother surface compared to QA–SNP, potentially due to the lower concentration of QA groups as a result of the dual functionalization with MBS1.

Elemental characterization conducted with EDS, as depicted in Fig. 3B, reveals varying carbon content across the coated surfaces. Uncoated and SNP-coated surfaces exhibit low to negligible carbon presence. In contrast, QA–SNP-coated surfaces display the highest percentage of carbon. Conversely, QA–MBS1–SNP-coated surfaces exhibit a lower carbon percentage, attributed to the reduced quantity of QA molecules present on the SNP surface. Similarly, the diminished carbon

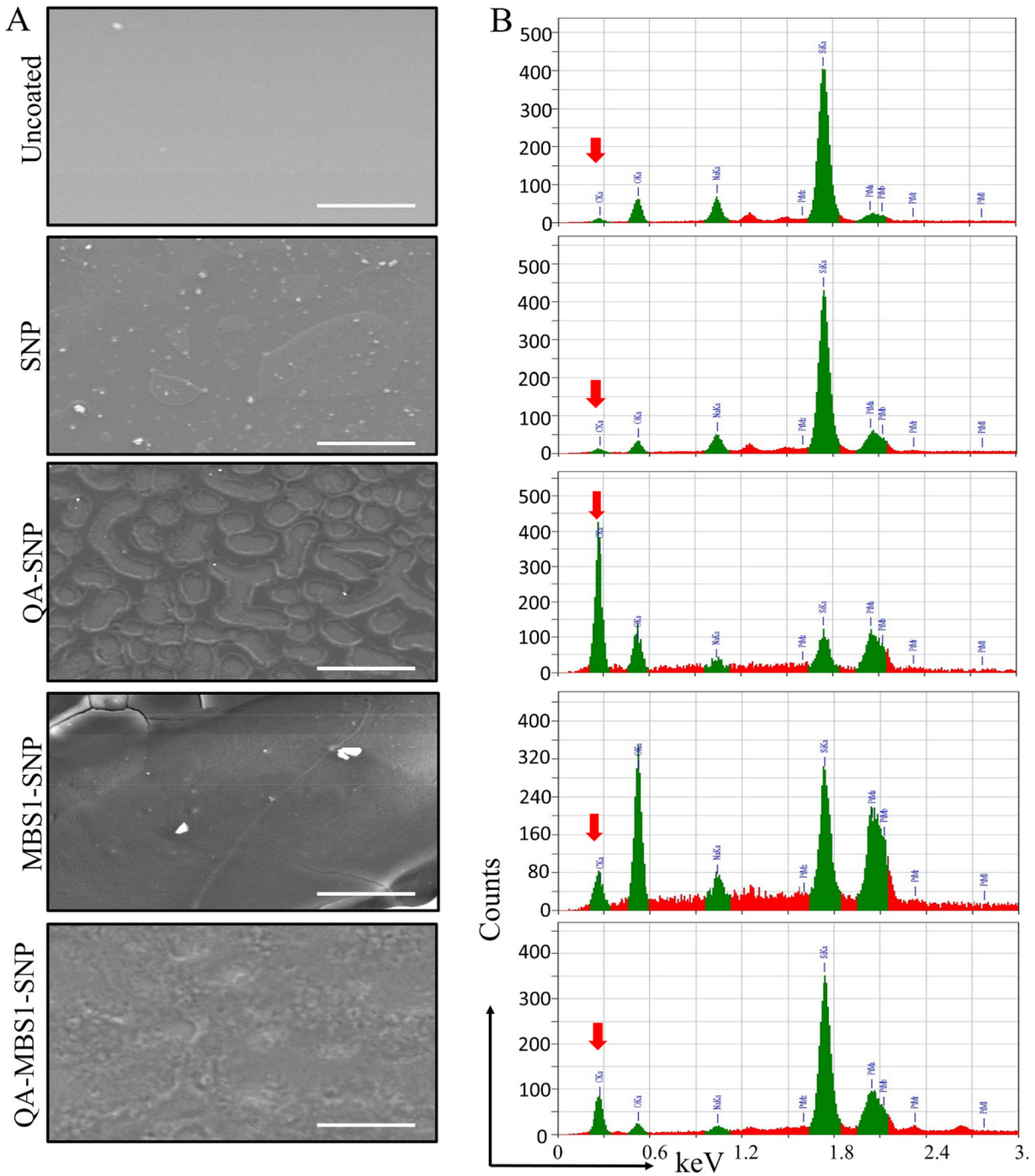

Fig. 3 Surface morphology studies: (A) SEM images showing the surface morphology of various coatings: SNP, QA–SNP, MBS1–SNP, and QA–MBS1–SNP, compared to an uncoated glass surface (scale bar 50 μm). (B) Corresponding Energy-Dispersive X-ray Spectroscopy (EDS) elemental analysis of the coatings. The analysis reveals increased carbon content in substrates coated with QAS and MBS1 compared to those with only SNP or the uncoated glass surface, indicating successful deposition of the coatings (note the red arrow highlighting the presence of carbon. Samples were sputter-coated with platinum).

content in MBS1–SNP-coated surfaces compared to QA–SNP coatings can be attributed to the lower number of carbons per molecule in MBS1 relative to QAS molecules.

MB exhibits maximum UV-Visible absorption at 660 nm.[38] The coated surfaces underwent characterization *via* UV-Visible spectral analysis to assess their absorption properties, with results presented in Fig. 4. Consistent with expectations, SNP and QA–SNP coated surfaces showed negligible light absorption at 660 nm. In contrast, both MBS1–SNP and QA–MBS1–SNP coated surfaces displayed a peak around 640–650 nm,

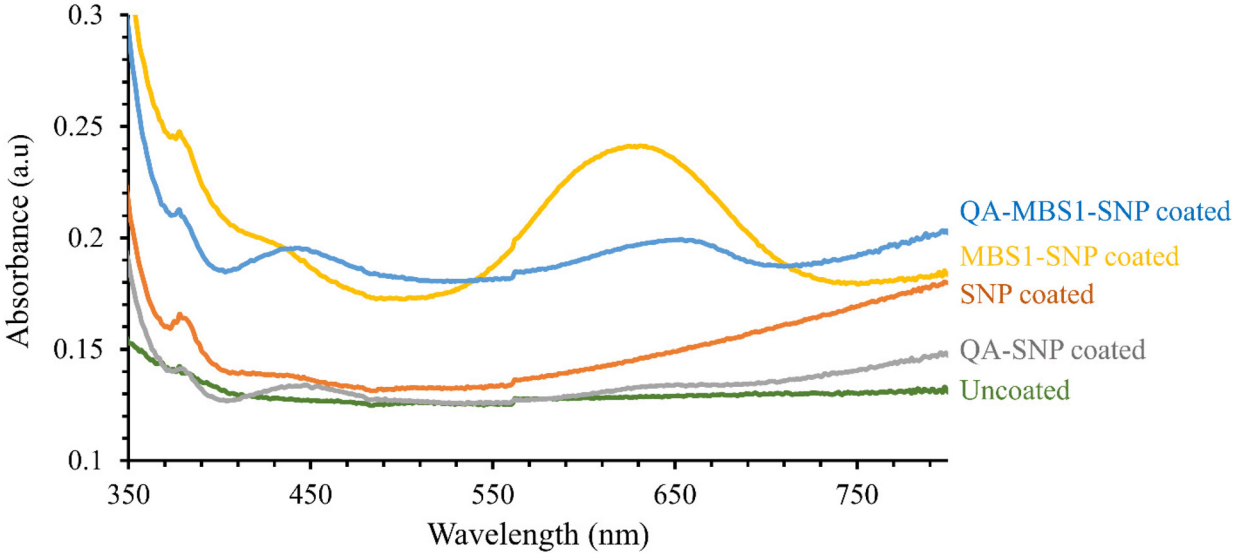

Fig. 4 UV-Visible absorption spectral analysis of uncoated, SNP, QA–SNP, MBS1–SNP, and QA–MBS1–SNP coated surfaces.

indicative of the presence of MB molecules. The UV-Visible absorbance was notably higher in MBS1–SNP coated glass slides compared to QA–MBS1–SNP, which possibly indicates a higher concentration of MB molecules per SNP. Nonetheless, it is crucial to emphasize that both MBS1–SNP and QA–MBS1–SNP coatings can serve as light-active surfaces owing to the incorporation of MB molecules within the coatings. Moreover, due to the covalent attachment of the MB molecule to the SNPs, no leakage of MB was observed when the surfaces were incubated with water for extended periods of time.

5.3. Bactericidal activity of surface coatings against *E. coli*

E. coli, known for its rapid growth and resilience towards disinfectants and antibacterial agents, is a prevalent pathogen on biomedical and healthcare surfaces.[39] Consequently, it served as the ideal test organism for assessing the bactericidal efficacy of these novel surface coatings. Our study involved exposing these coatings to *E. coli* under light and dark conditions (as shown in SFig. 2.†) to investigate their ability to kill *E. coli* over short time exposure, thereby preventing their growth and reproduction. The maintained lux value of ~500 lux (~0.0732 mW cm^{-2}) for light exposure experiments was chosen for all *a*PDT experiments to reflect typical workplace lighting conditions in healthcare settings.

Fig. 5A and B illustrates the bactericidal activity of uncoated and various SNP surface coatings against *E. coli*. Following a 30 minute incubation period in dark or white light conditions, viable bacterial counts were determined by subculturing samples collected from the contaminated surfaces (Fig. 5A). Uncoated, SNP, and QA–SNP coated surfaces exhibited high bacterial viability both in the presence and absence of white light treatments, as expected due to their lack of light activation. Conversely, while bacterial survival was observed in the absence of light exposure, almost no *E. coli* survived even with short-term exposure to white light on the MBS1–SNP and QA–MBS1–SNP coated surfaces. This can be attributed to the *a*PDT activity of these surfaces against *E. coli* microorganisms. The bacterial population reduction following the bactericidal test was represented by a logarithmic reduction factor in (Fig. 5B). The results revealed that uncoated, SNP-coated, and QA–SNP coated surfaces displayed less than a 2-log reduction in bacterial counts, irrespective of light exposure. Additionally, no significant difference was observed in the bactericidal activity between dark and light conditions for these coatings.

Conversely, MBS1–SNP and QA–MBS1–SNP coated surfaces demonstrated statistically significant (*t*-test $p^* < 0.05$ and $p^{**} < 0.01$) reductions in viable bacteria (~5-log reduction, equivalent to a 99.999% reduction rate) when exposed to white light compared to uncoated, SNP, and QA–SNP coated surfaces. Notably, MBS1–SNP coated surfaces exhibited over a 2-log reduction in bacterial population in the dark, suggesting inherent toxicity towards *E. coli*. The cationic structure, hydrophilic, and the redox nature of MB facilitate greater interaction with Gram negative *E. coli*, leading to damage to the outer cellular membrane.[40,41] Both surface coatings displayed decreased bacterial survival rates when exposed to white light compared to dark conditions, indicative of surface phototoxicity. Light exposure initiated the photo-bactericidal activity of MB, releasing cytotoxic singlet oxygen species that caused oxidative damage to the outer cell membrane of *E. coli*, leading to cell death. The decreased bactericidal activity of QA–MBS1–SNP coated surfaces (4.34-log reduction) compared to MBS1–SNP surfaces (5.65-log reduction) in the presence of light might be due to the higher loading of MBS1 molecules per SNP particle in MBS1–SNP, leading to increased generation of reactive oxygen species compared to QA–MBS1–SNP. The dual functionalization with QA could potentially reduce the

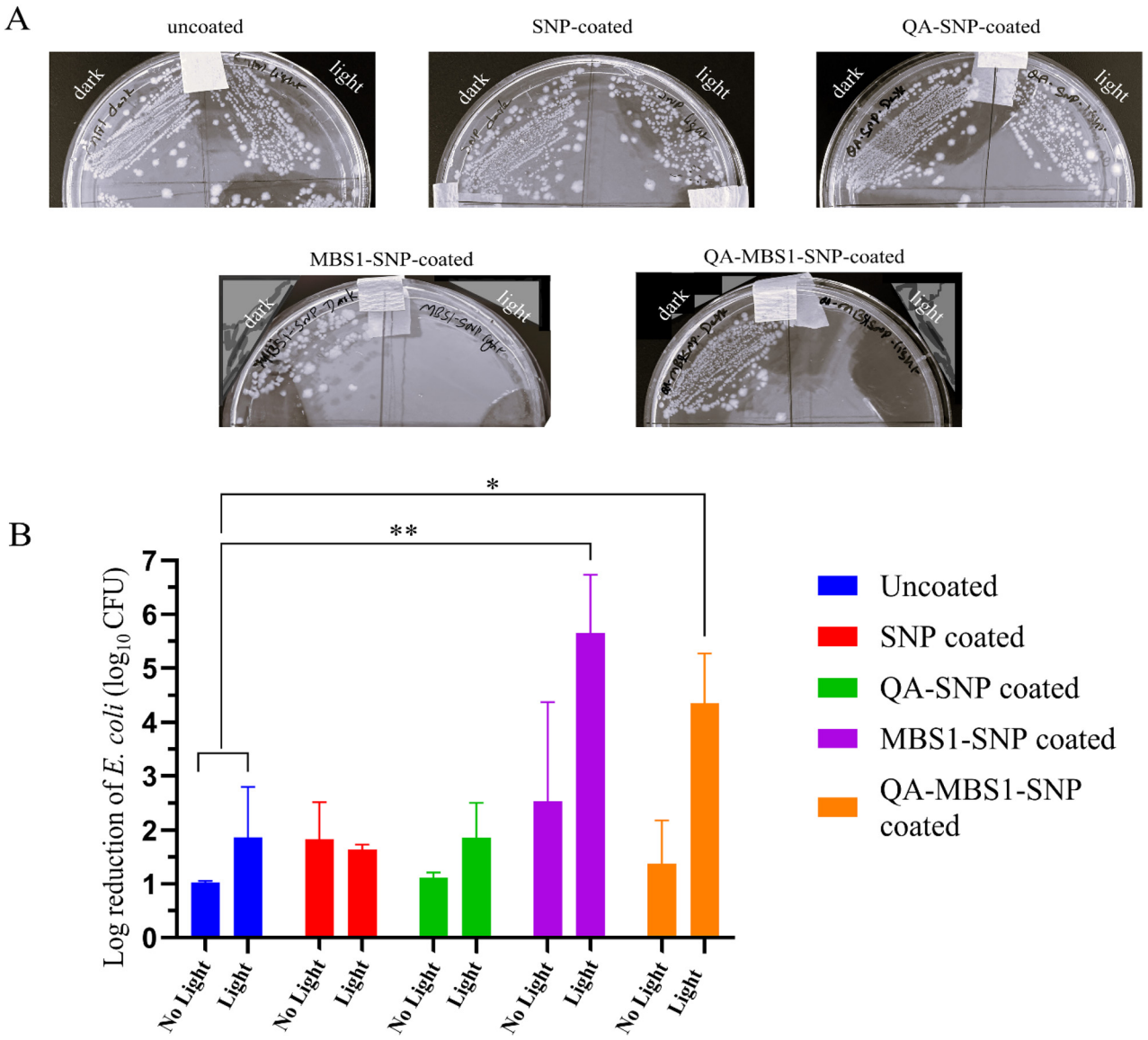

Fig. 5 Bactericidal activity of uncoated, SNP, QA–SNP, MBS1–SNP, and QA–MBS1–SNP coated surfaces after short time incubation of 30 minutes, in the presence and absence of white light (~500 lux (~0.0732 mW cm^{-2})). (A) Viable E, coli bacteria by subculturing samples collected from the contaminated surfaces. (B) Graphical representation of Log reduction of *E. coli* after short-term exposure to coated surfaces. MBS1–SNP coated, and QA–MBS1–SNP coated surfaces significantly reduced the bacterial viability in presence of white light upon short-term exposure. Unpaired Student's *t*-test and one-way ANOVA used to compare between groups: * for $p < 0.05$, ** for $p < 0.01$.

encapsulation of MBS1 per nanoparticle. These findings suggest that the *a*PDT activity significantly enhances bactericidal efficacy.

Additionally, the surface morphology of *E. coli* observed using TEM, after incubation with these surface coatings and light exposure are shown in Fig. 6. The bacteria collected from the uncoated and SNP-coated surfaces appeared no visible damage to the outer membrane. However, disruption of the outer cell wall was observed in samples collected from QA–SNP coated surfaces, indicating some level of damage. More pronounced damage was evident in cells collected from MBS1–SNP and QA–MBS1–SNP coated surfaces, suggesting a more efficient and immediate cell killing action following *a*PDT treatment. These observations underscore the effectiveness of *a*PDT in inducing cellular damage and highlight the potential phototoxicity of MB-containing coatings in combating bacterial pathogens.

5.4. Assessment of *E. coli* biofilm inhibition on coated glass substrates after long term incubation

After incubation of *E. coli* with various SNP-coated substates for extended periods of time (up to 48 hours) in the absence and presence of white light, the bacterial adherence capacity, biofilm formation, and morphology changes were examined using SEM imaging. Fig. 7A and B illustrate the SEM images, revealing dense bacterial colonies aggregating and forming complex biofilms on the uncoated surface both in dark and

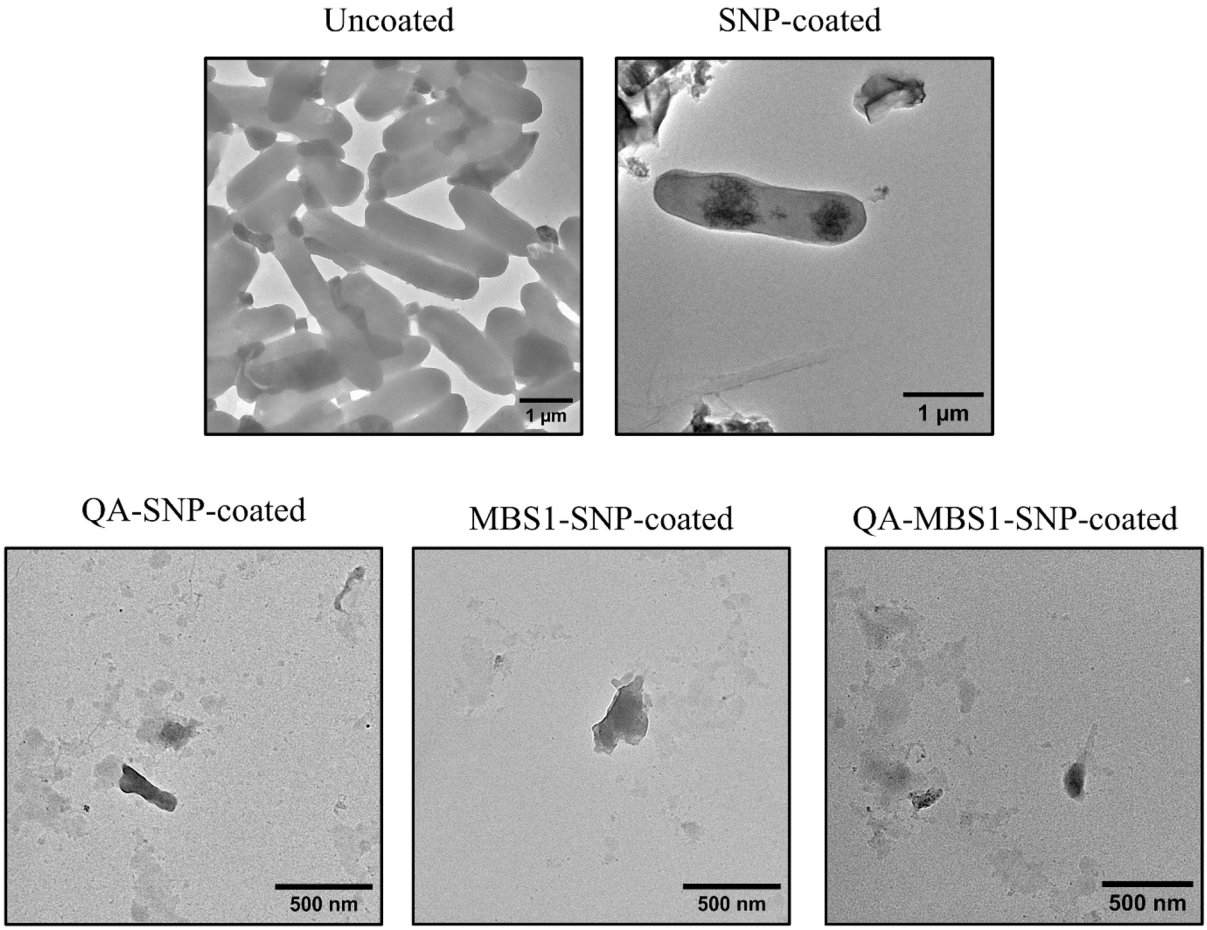

Fig. 6 TEM images of photodamaged samples collected from uncoated, SNP, QA–SNP, MBS1–SNP and QA–MBS1–SNP coated surfaces 30 minutes after light treatment. The collected samples displayed undamaged bacteria from uncoated and SNP-coated surfaces whereas, damaged outer cellular membrane and arrest of bacterial cell growth were noticed in samples collected from QA–SNP, MBS1–SNP, and QA–MBS1–SNP coated surfaces due to contact killing activity and aPDT (scale bar 1 μm for uncoated and SNP-coated, 500 nm in QA–SNP, MBS1–SNP, and QA–MBS1–SNP coated).

light conditions. The biofilm formation on SNP coated surfaces was found to be comparable to that on uncoated surfaces, with no significant reduction in bacterial adherence or biofilm formation. In addition, the outer membrane walls of bacteria were undisturbed and undamaged when grown on uncoated and SNP-coated surfaces. On the QA–SNP coated surfaces, a thick layer of *E. coli* biofilm was observed after prolonged incubation, irrespective of the light conditions. This finding contradicts previous literature reports that highlight the contact-killing and anti-biofouling properties of QA-coated surfaces.[23,42,43] The observed ineffectiveness of QA–SNP coatings against *E. coli* might be due to the specific coating methodology used in this study. Notably, the SEM images revealed that bacteria on QA–SNP coated surfaces exhibited rough, wrinkled, and ruptured membranes with noticeable holes. This suggests that the QA–SNP coatings may induce bacterial membrane damage through electrostatic interactions between the positively charged QAS and the negatively charged bacterial cell membranes. However, the cationic nature of QAS may render these surfaces more susceptible to biofouling due to the adhesion of anionic compounds in organic matter, potentially enhancing bacterial adhesion on QA–SNP coated surfaces. The extent of bacterial adhesion could potentially be modulated by adjusting the concentration of QAS during the synthesis of QA–SNP nanoparticles for surface coatings. However, for the purposes of this study, we opted to maintain a constant QAS concentration.

Interestingly, a notable reduction in biofilm formation was observed on both MBS1–SNP and QA–MBS1–SNP coated surfaces, even in the absence of light. This reduction might be due to the intrinsic antimicrobial activity of MB, which has been reported to compromise the viability of *E. coli*.[44] Despite diminished biofilm formation, viable bacteria on these surfaces under dark conditions exhibited normal growth and appeared healthy. However, when exposed to white light, the bacterial cultures on these surfaces demonstrated marked changes. The bacteria exhibited signs of photodamage, such as parched cell walls and significant morphological alterations. Specifically, the application of *aPDT* led to a disruption of the bacterial outer membrane, resulting in the loss of intra-

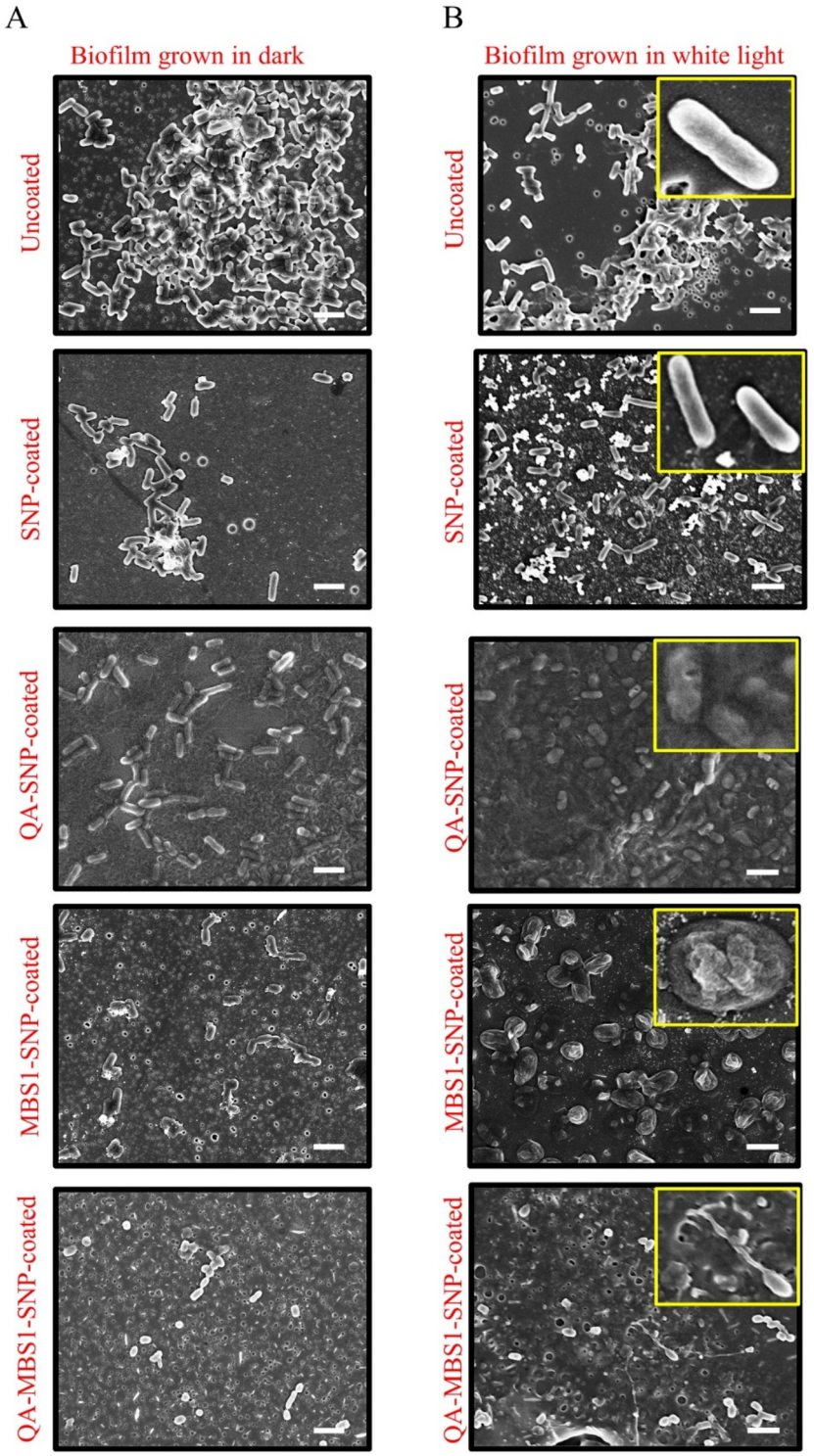

Fig. 7 (A and B) SEM images of bacteria, grown on uncoated, SNP, and QA–SNP, MBS1–SNP, and QA–MBS1–SNP in presence of dark and white light (scale bar 2 μm).

cellular components. Additionally, *a*PDT induced a transformation in *E. coli* morphology from bacilli (rod shaped) to cocci (spherical), consistent with the effects documented in previous studies on *a*PDT impact on biofilms.[45–47] Despite the reduction in viable bacteria on MBS1–SNP coated surfaces, some bacteria remained adherent to the surfaces in an inactivated state, indicating residual surface affinity. Conversely, QA–MBS1–SNP coated surfaces exposed to white light exhibited a further reduction in bacterial adhesion, with fewer colonies adhering to the surface and the majority appearing as

single-cell entities. This enhanced antibiofouling effect suggests that the incorporation of QA in the coating not only improves the efficacy of *a*PDT but also enhances the overall resistance to bacterial colonization. The combination of MB with QA in the coatings significantly improved the antibacterial and antibiofouling properties by rapidly affecting bacterial viability upon contact, particularly when exposed to light.

To quantify the amount of biofilm formed, CV assay was conducted. As depicted in Fig. 8A, both MBS1–SNP and QA–MBS1–SNP coated surfaces exhibited significant potency in inhibiting biofilm formation. Particularly noteworthy was the substantial reduction in biofilm formation observed when exposed samples were subjected to white light treatment (*a*PDT). Both samples demonstrated a significant (*t*-test $p^* < 0.05$ and $p^{**} < 0.01$) decrease in biofilm formation compared to the control sample. On the other hand, SNP and QA–SNP coated surfaces showed less antibiofouling activity, due to the lack of *a*PDT activity. However, these surfaces showed antibacterial resistance compared to uncoated surfaces, despite not exhibiting bactericidal activity in the earlier experiments. This discrepancy may stem from the prolonged exposure of bacterial samples to the coated surfaces. In previous assessments of bactericidal activity, *E. coli* cultures were exposed to the coated surfaces for only a short duration (30 minutes).

The presence of biofilm formation on the coated surfaces was further confirmed through fluorescence imaging using acridine orange (AO) as a stain. Glutaraldehyde-fixed and AO-stained samples were visualized using confocal microscopy at

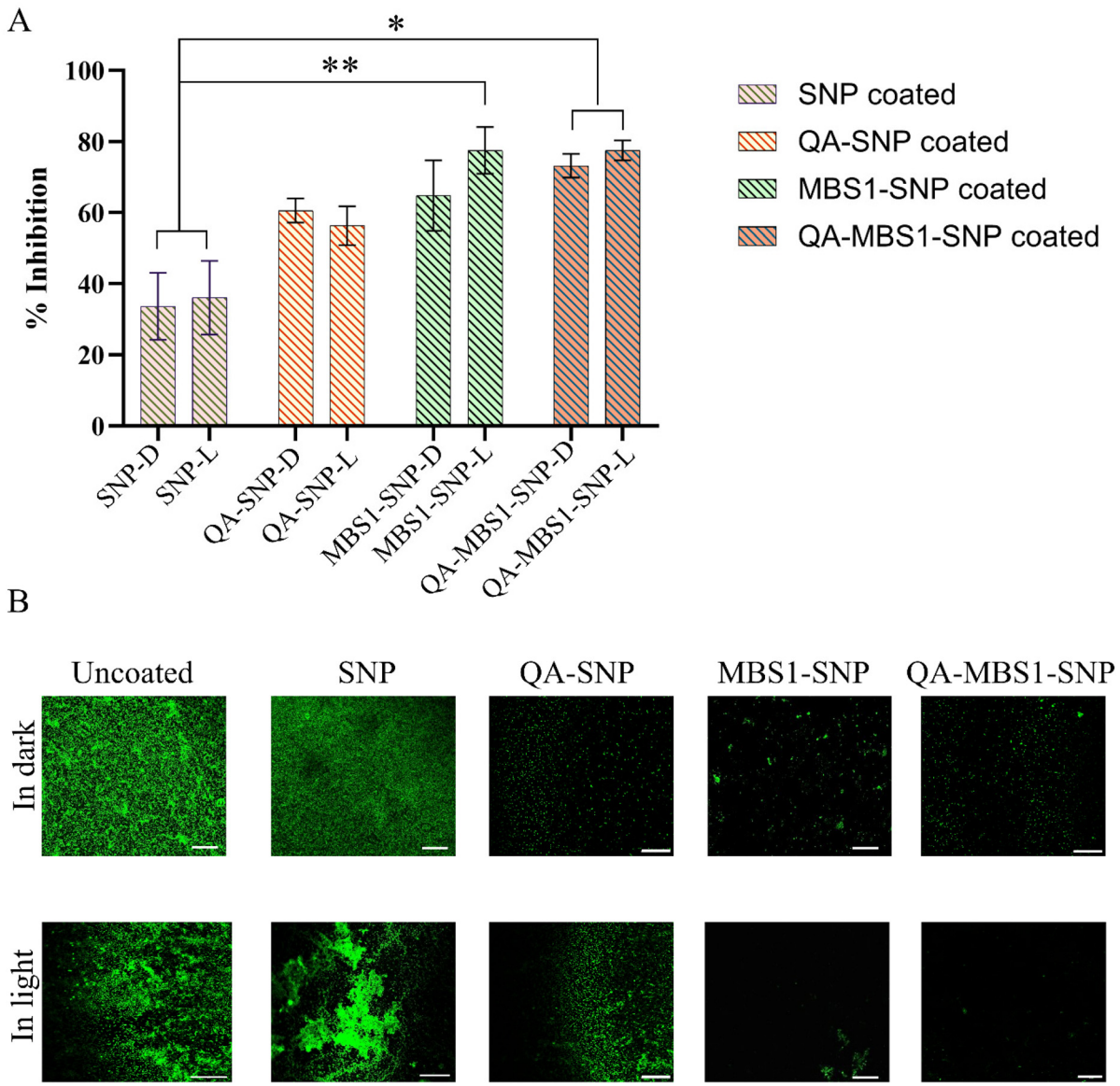

Fig. 8 Biofilm inhibition tests: (A) CV assay performed to quantify the adhered bacteria on the surfaces and (B) biofilms visualization using fluorescence imaging (scale bar 50 μm) (two-tailed Student's *t*-test $*p < 0.05$, $**p < 0.01$).

a wavelength of 525 nm (Fig. 8B). The results revealed a dense layer of thick biofilm formed on both uncoated and SNP-coated surfaces under both light and dark conditions. The QA-coated surfaces also showed bacterial adhesion onto the surfaces; however, no substantial formation of thick biofilm colonies was observed. In contrast, MBS1–SNP and QA–MBS1–SNP coated surfaces exhibited significantly less biofilm growth compared to the control samples and the effect was more pronounced when exposed to white light compared to culture grown in dark conditions, consistent with the SEM and CV results.

6. Conclusion and future outlook

In summary, this study developed dual-action antimicrobial and antibiofouling surface coatings by covalently incorporating MBS1 and QAS into silica nanoparticles. QA–SNP coatings exhibited excellent hydrophobicity, enhancing bacterial repellence, while MBS1–SNP coatings demonstrated potent photokilling activity. The combined QA–MBS1–SNP coatings successfully integrated both photokilling and bacterial repellence functionalities, addressing the issue of dye leakage through covalent incorporation of MBS1 into SNPs. This ensured sustained antimicrobial activity. Preliminary tests against *E. coli* revealed the superior dual efficacy of QA–MBS1–SNP coatings. In addition to the phototoxic effects of MBS1, these coatings induced hydrophobicity, further enhancing antibiofouling properties. These findings highlight the potential of light-activated surface coatings in controlling biofilm formation and mitigating microbial infections, offering a compelling alternative for healthcare, industrial, and environmental applications.

Future work should focus on evaluating the performance of these coatings against a broader spectrum of microorganisms, including clinically relevant pathogens. Moreover, studies assessing the coating's durability, photostability, and long-term performance under real-world conditions will be critical for advancing their practical application. Incorporating this technology into diverse substrates and exploring scalable manufacturing methods will also be essential for translating these coatings from the laboratory to commercial use. By addressing these challenges, the dual-action antimicrobial and antibiofouling coatings hold significant promise in combating microbial contamination and biofilm-associated risks on a global scale.

Author contributions

Haritha Kirla: Conceptualization, methodology, investigation, writing – original draft. David J. Henry: Conceptualization, resources, writing – review & editing, supervision. Zhong-Tao Jiang: Resources, writing – review & editing, supervision. Juliana Hamzah: Resources, writing – review & editing, supervision. All authors have given approval to the final version of the manuscript.

Data availability

Data will be made available on request.

Conflicts of interest

The authors declare no competing financial interest.

Acknowledgements

This research was supported by an Australian Government Research Training Program (RTP) scholarship. The authors like to acknowledge the Microscopy Australia (ROR: 042mm0k03) at the Centre for Microscopy, Characterisation and Analysis, the University of Western Australia, enabled by NCRIS.

References

1 M. J. Lydeamore, B. G. Mitchell, T. Bucknall, A. C. Cheng, P. L. Russo and A. J. Stewardson, Burden of five healthcare associated infections in Australia, *Antimicrob. Resist. Infect. Control*, 2022, **11**(1), 69.
2 Australian Commission on Safety and Quality in Health Care. NSQHS Standards 2021 Preventing and Controlling Infections Standard [Internet]. Available from: **https://www.safetyandquality.gov.au/publications-and-resources/resource-library/nsqhs-standards-2021-preventing-and-controlling-infections-standard**.
3 Australian commission on safety and quality in health care. HEALTHCAREASSOCIATED INFECTIONS [Internet]. Available from: **https://www.safetyandquality.gov.au/sites/default/files/migrated/Healthcare-associated-infection-detailed-fact-sheet.pdf**.
4 R. F. O'Toole, The interface between COVID-19 and bacterial healthcare-associated infections, *Clin. Microbiol. Infect.*, 2021, **27**(12), 1772–1776.
5 L. Wang, C. Hu and L. Shao, The antimicrobial activity of nanoparticles: present situation and prospects for the future, *Int. J. Nanomed.*, 2017, **12**, 1227–1249.
6 C. Spagnul, L. C. Turner and R. W. Boyle, Immobilized photosensitizers for antimicrobial applications, *J. Photochem. Photobiol., B*, 2015, **150**, 11–30.
7 T. Walker, M. Canales, S. Noimark, K. Page, I. Parkin, J. Faull, *et al.*, A Light-Activated Antimicrobial Surface Is Active Against Bacterial, Viral and Fungal Organisms, *Sci. Rep.*, 2017, **7**(1), 15298.
8 C. R. Ghareeb, B. S. T. Peddinti, S. C. Kisthardt, F. Scholle, R. J. Spontak and R. A. Ghiladi, Toward Universal Photodynamic Coatings for Infection Control, *Front. Med.*, 2021, **8**, 657837.
9 T. Ameh, K. Zarzosa, W. E. Braswell and C. M. Sayes, Nanoparticle surface coatings produce distinct antibacter-

ial effects that are consistent across diverse bacterial species, *Front. Toxicol.*, 2023, **5**, 1119547.

10 D. Kışla, G. G. Gökmen, G. Akdemir Evrendilek, T. Akan, T. Vlčko, P. Kulawik, *et al.*, Recent developments in antimicrobial surface coatings: Various deposition techniques with nanosized particles, their application and environmental concerns, *Trends Food Sci. Technol.*, 2023, **135**, 144–172.

11 S. P. Songca and Y. Adjei, Applications of Antimicrobial Photodynamic Therapy against Bacterial Biofilms, *Int. J. Mol. Sci.*, 2022, **23**(6), 3209.

12 X. Hu, H. Zhang, Y. Wang, B. C. Shiu, J. H. Lin, S. Zhang, *et al.*, Synergistic antibacterial strategy based on photodynamic therapy: Progress and perspectives, *Chem. Eng. J.*, 2022, **450**, 138129.

13 S. Noimark, E. Allan and I. P. Parkin, Light-activated antimicrobial surfaces with enhanced efficacy induced by a dark-activated mechanism, *Chem. Sci.*, 2014, **5**(6), 2216–2223.

14 P. Parasuraman, A. P. Antony, B. Sruthil Lal S, A. Sharan, B. Siddhardha, K. Kasinathan, *et al.*, Antimicrobial photodynamic activity of toluidine blue encapsulated in mesoporous silica nanoparticles against *Pseudomonas aeruginosa* and *Staphylococcus aureus*, *Biofouling*, 2019, **35**(1), 89–103.

15 K. Liu, Y. Luo, L. Hao and J. Chen, Antimicrobial effect of methylene blue in microbiologic culture to diagnose periprosthetic joint infection: an in vitro study, *J. Orthop. Surg. Res.*, 2022, **17**(1), 571.

16 P. Parasuraman, R. Y. Thamanna, C. Shaji, A. Sharan, A. H. Bahkali, H. F. Al-Harthi, *et al.*, Biogenic Silver Nanoparticles Decorated with Methylene Blue Potentiated the Photodynamic Inactivation of Pseudomonas aeruginosa and Staphylococcus aureus, *Pharmaceutics*, 2020, **12**(8), 709.

17 K. A. Vos, P. M. K. Gordon and B. Heyne, Methylene blue in combination with sunlight as a low cost and effective disinfection method for coronavirus-contaminated PPE, *Am. J. Infect. Control*, 2022, **50**(8), 906–908.

18 A. Fouda, S. E. D. Hassan, A. M. Eid, M. A. Abdel-Rahman and M. F. Hamza, Light enhanced the antimicrobial, anticancer, and catalytic activities of selenium nanoparticles fabricated by endophytic fungal strain, Penicillium crustosum EP-1, *Sci. Rep.*, 2022, **12**(1), 11834.

19 M. Mirzahosseinipour, K. Khorsandi, R. Hosseinzadeh, M. Ghazaeian and F. K. Shahidi, Antimicrobial photodynamic and wound healing activity of curcumin encapsulated in silica nanoparticles, *Photodiagn. Photodyn. Ther.*, 2020, **29**, 101639.

20 H. Kirla, D. J. Henry, S. Jansen, P. L. Thompson and J. Hamzah, Use of Silica Nanoparticles for Drug Delivery in Cardiovascular Disease, *Clin. Ther.*, 2023, **45**(11), 1060–1068.

21 C. Piccirillo, S. Perni, J. Gil-Thomas, P. Prokopovich, M. Wilson, J. Pratten, *et al.*, Antimicrobial activity of methylene blue and toluidine blue O covalently bound to a modified silicone polymer surface, *J. Mater. Chem.*, 2009, **19**(34), 6167.

22 D. Diaz, J. Church, M. Young, K. T. Kim, J. Park, Y. B. Hwang, *et al.*, Silica-quaternary ammonium "Fixed-Quat" nanofilm coated fiberglass mesh for water disinfection and harmful algal blooms control, *J. Environ. Sci.*, 2019, **82**, 213–224.

23 J. M. Boyce, Quaternary ammonium disinfectants and antiseptics: tolerance, resistance and potential impact on antibiotic resistance, *Antimicrob. Resist. Infect. Control*, 2023, **12**(1), 32.

24 M. J. Saif, J. Anwar and M. A. Munawar, A Novel Application of Quaternary Ammonium Compounds as Antibacterial Hybrid Coating on Glass Surfaces, *Langmuir*, 2009, **25**(1), 377–379.

25 H. Kirla and D. J. Henry, Synthesis and characterization of novel silane derivatives of phenothiazinium photosensitisers, *Dyes Pigm.*, 2022, **199**, 110087.

26 H. Kirla, J. Wu, J. Hamzah and D. J. Henry, One-pot synthesis and covalent conjugation of methylene blue in mesoporous silica nanoparticles – a platform for enhanced photodynamic therapy, *Colloids Surf., B*, 2024, 114195.

27 G. B. Hwang, H. Huang, G. Wu, J. Shin, A. Kafizas, K. Karu, *et al.*, Photobactericidal activity activated by thiolated gold nanoclusters at low flux levels of white light, *Nat. Commun.*, 2020, **11**(1), 1207.

28 P. Paramanantham, B. Siddhardha, S. B. S. Lal, A. Sharan, A. A. Alyousef, M. S. Al Dosary, *et al.*, Antimicrobial photodynamic therapy on *Staphylococcus aureus* and *Escherichia coli* using malachite green encapsulated mesoporous silica nanoparticles: an *in vitro* study, *PeerJ*, 2019, **7**, e7454.

29 H. Taha, D. J. Henry, C. Y. Yin, A. Amri, X. Zhao, S. Bahri, *et al.*, Probing the effects of thermal treatment on the electronic structure and mechanical properties of Ti-doped ITO thin films, *J. Alloys Compd.*, 2017, **721**, 333–346.

30 M. Hassen, R. Riahi, F. Laatar and H. Ezzaouia, Optical and surface properties of CdSe thin films prepared by sol-gel spin coating method, *Surf. Interfaces*, 2020, **18**, 100408.

31 S. D. Chandradoss, A. C. Haagsma, Y. K. Lee, J. H. Hwang, J. M. Nam and C. Joo, Surface Passivation for Single-molecule Protein Studies, *J. Visualized Exp.*, 2014, **86**, 50549.

32 P. Q. T. Do, V. T. Huong, N. T. T. Phuong, T. H. Nguyen, H. K. T. Ta, H. Ju, *et al.*, The highly sensitive determination of serotonin by using gold nanoparticles (Au NPs) with a localized surface plasmon resonance (LSPR) absorption wavelength in the visible region, *RSC Adv.*, 2020, **10**(51), 30858–30869.

33 J. X. H. Wong and H. Z. Yu, Preparation of Transparent Superhydrophobic Glass Slides: Demonstration of Surface Chemistry Characteristics, *J. Chem. Educ.*, 2013, **90**(9), 1203–1206.

34 R. Sukarsono, M. Rachmawati, S. R. Susilowati, D. Husnurrofiq, K. Nurwidyaningrum and A. K. Dewi, Effect of Sol Concentration, Aging and Drying Process on Cerium Stabilization Zirconium Gel Produced by External Gelation, *J. Phys.:Conf. Ser.*, 2018, **962**, 012056.

35 D. Sriramulu, E. L. Reed, M. Annamalai, T. V. Venkatesan and S. Valiyaveettil, Synthesis and Characterization of

Superhydrophobic, Self-cleaning NIR-reflective Silica Nanoparticles, *Sci. Rep.*, 2016, **6**(1), 35993.

36 M. Zainuri, W. Dini Putri and A. S. Bintoro, Hydrophobicity of tetraethyl-orthosilicate-derived silica coating at various concentrations, *J. Phys.:Conf. Ser.*, 2021, **1951**(1), 012021.

37 Y. Lou, D. Schapman, D. Mercier, S. Alexandre, F. Burel, P. Thebault, *et al.*, Self-disinfecting PDMS surfaces with high quaternary ammonium functionality by direct surface photoinitiated polymerization of vinylbenzyl dimethyl-butylammonium chloride, *Eur. Polym. J.*, 2021, **152**, 110473.

38 M. Wainwright and K. B. Crossley, Methylene Blue - a Therapeutic Dye for All Seasons?, *J. Chemother.*, 2002, **14**(5), 431–443.

39 S. Arbab, H. Ullah, W. Wang and J. Zhang, Antimicrobial drug resistance against *Escherichia coli* and its harmful effect on animal health, *Vet. Med. Sci.*, 2022, **8**(4), 1780–1786.

40 M. Smolinskáa and A. Takáčováa, Effect of photoactive dye on bacteria contained in activated sludge, *Acta Chim. Slovaca*, 2012, **5**(2), 164–168.

41 M. N. Usacheva, M. C. Teichert and M. A. Biel, Comparison of the methylene blue and toluidine blue photobactericidal efficacy against gram–positive and gram–negative microorganisms, *Lasers Surg. Med.*, 2001, **29**(2), 165–173.

42 L. Bastarrachea, D. Wong, M. Roman, Z. Lin and J. Goddard, Active Packaging Coatings, *Coatings*, 2015, **5**(4), 771–791.

43 I. Mukherjee, A. Ghosh, P. Bhadury and P. De, Side-Chain Amino Acid-Based Cationic Antibacterial Polymers: Investigating the Morphological Switching of a Polymer-Treated Bacterial Cell, *ACS Omega*, 2017, **2**(4), 1633–1644.

44 K. Liu, Y. Luo, L. Hao and J. Chen, Antimicrobial effect of methylene blue in microbiologic culture to diagnose peri-prosthetic joint infection: an in vitro study, *J. Orthop. Surg. Res.*, 2022, **17**(1), 571.

45 A. S. Garcez, M. Kaplan, G. J. Jensen, F. R. Scheidt, E. M. Oliveira and S. S. Suzuki, Effects of antimicrobial photodynamic therapy on antibiotic-resistant Escherichia coli, *Photodiagn. Photodyn. Ther.*, 2020, **32**, 102029.

46 K. Huang, J. Wang, A. Zhuang, Q. Liu, F. Li, K. Yuan, *et al.*, Metallacage-based enhanced PDT strategy for bacterial elimination via inhibiting endogenous NO production, *Proc. Natl. Acad. Sci. U. S. A.*, 2023, **120**(29), e2218973120.

47 A. S. Garcez, S. C. Núñez, N. Azambuja, E. R. Fregnani, H. M. H. Rodriguez, M. R. Hamblin, *et al.*, Effects of Photodynamic Therapy on Gram-positive and Gram-negative Bacterial Biofilms by Bioluminescence Imaging and Scanning Electron Microscopic Analysis, *Photomed. Laser Surg.*, 2013, **31**(11), 519–525.